# Reactive Power Compensator Control for Power Factor Improvement Using the Internet of Things

*Fandi Muhammad[a], Ayusta Lukita Wardani[b], Aditya Candra Hermawan[c], Nur Vidia Laksmi[d]*

[a,b,c,d] *Department of Electrical Engineering, Vocational Faculty, Universitas Negeri Surabaya, Indonesia*

ARTICLE INFO

*Article history:*
Received January 22, 2026
Received in revised form
May 10, 2024
Accepted June 21, 2026
Available online June 30, 2026

*Keywords:*
Internet of Things
Power Factor
Reactive Power Compensation
Three-phase System

ABSTRACT

*A low power factor caused by inductive loads remains a major issue in electrical distribution systems, leading to an increased reactive power demand and reduced energy efficiency. This study proposes the design and implementation of a three-phase reactive power compensator integrated with Internet of Things (IoT) technology to improve the power factor automatically and in real time. The system employs three PZEM-004T sensors to measure the electrical parameters in each phase, an Arduino Mega 2560 as the main controller, and an ESP32 module for wireless communication with a Firebase real-time database. A mobile monitoring and control interface was developed using the MIT App Inventor, enabling remote access through Android devices. The capacitor bank consists of nine capacitor units arranged as 6.5 µF, 4.0 µF, and 3.5 µF for each phase, which are automatically switched via relays based on the detected power factor and reactive power compensation requirement. Experimental testing under laboratory-scale balanced three-phase fluorescent lamp loads showed that the proposed system improved the power factor from an initial range of 0.43–0.44 to 0.90–0.93 after compensation. The system response time ranged from 2–9 s under static load conditions, 6–12 s during dynamic load changes under compensation, and 1–16 s under over-compensation conditions. The longer response time in the overcompensation test occurred during transitions that required capacitor disconnection and re-selection of the appropriate capacitor combination. The IoT-based monitoring system was evaluated by comparing the PZEM-004T readings with those of a conventional power quality analyzer, Lutron DW-6095. The measurement differences ranged from 0.4–1.1 V for voltage, 0.00–0.03 A for current, and 0.00–0.03 for the power factor. The corresponding percentage errors were 0.17–0.47%, 0.0–9.7 %, and 0.0–5.0% for voltage, current, and power factor, respectively. The results demonstrate that the proposed IoT-based reactive power compensator is effective in improving the power factor and enabling the remote monitoring of electrical parameters in a three-phase low-voltage system.*

## 1 Introduction

Electrical power quality is an important aspect of modern power systems, particularly in distribution networks dominated by inductive loads, such as electric motors, transformers, and fluorescent lamps. Inductive loads cause a phase shift between the voltage and current, thereby reducing the power factor. A low power factor increases power losses, reduces system efficiency, and causes excessive loading on distribution networks and electrical equipment [1][2].

Power factor correction is commonly performed through reactive power compensation using capacitor banks (CBs). Capacitors produce capacitive reactive power that can compensate for the inductive reactive power of the load, allowing the power factor to be increased toward unity [3]. Several studies [4][5][6] have shown that automatic capacitor bank systems can significantly improve the power factor and reduce power losses in electrical power systems. However, conventional compensation systems are generally local and require manual adjustment, making them less flexible in responding to dynamic load variations.

The development of Internet of Things (IoT) technology has provided new opportunities for electrical monitoring and control systems. IoT enables real-time acquisition of electrical parameter data and remote device control through an internet network [7]. Previous research [8] showed that an IoT-based power factor monitoring system using the PZEM-004T sensor can effectively improve the power factor and provide online monitoring of electrical parameters. However, that study was limited to a single-phase system and did not accommodate the needs of three-phase systems, which are commonly used in industrial installations and medium-scale electrical systems.

Another study [9] developed a microcontroller-based automatic capacitor bank for power factor correction, but the proposed system was not integrated with an IoT platform, so monitoring and control were still limited to a local area. Based on these limitations, an IoT-based reactive power compensator is required that can operate on a three-phase network, provide real-time monitoring capability, and control capacitors automatically and remotely.

Therefore, this study aims to design and implement a three-phase reactive power compensator control system based on Internet of Things (IoT) technology to improve the power factor automatically and in real time. The system uses PZEM-004T sensors for electrical parameter measurements, a microcontroller as the controller, and a cloud platform as the monitoring and control medium. The proposed system is expected to improve electrical energy efficiency, enhance power quality, and provide a more flexible and modern solution for the reactive power management.

## 2 Literature Study

### *2.1. Active Power*

Real power or active power is the power consumed to perform useful work. This power is the basis for electricity billing recorded by the kWh meter and is expressed in watts (W) [10]. In an alternating-current system with a per-phase measurement, the active power can be calculated using the following equation:

$$P = V \,.\, I \,.\, \cos \varphi \qquad (1)$$

Description: P = active power per phase (W)
V = voltage (V)
I = current (A)
cos φ = power factor

In this study, the electrical parameters were measured for each phase using PZEM-004T sensors. Therefore, the total active power of the three-phase system can be calculated from the sum of the active powers of each phase, as shown in the following equation:

Corresponding Author: fandimuhammadyt@gmail.com

Doi : 10.30996/elsains.v8i1.133178

$$P_{Total} = P_R + P_S + P_T \quad (2)$$

Description: $P_{Total}$ = total active power (W)
$P_R$ = active power of phase R (W)
$P_S$ = active power of phase S (W)
$P_T$ = active power of phase T (W)

### 2.2. Reactive Power

Reactive power arises from the formation of a magnetic field in inductive loads. The unit of reactive power is volt-ampere reactive (VAR). Reactive power can be defined as the product of voltage, current, and sin φ [11]. In the per-phase measurement, the reactive power can be calculated using the following equation:

$$Q = V \,.\, I \,.\, \sin\varphi \quad (3)$$

Description: Q = reactive power per phase (VAR)
V = voltage n (V)
I = current (A)
$\sin\varphi$ = reactive factor

The total reactive power is obtained from the sum of the reactive power of each phase, as shown in the following equation:

$$Q_{Total} = Q_R + Q_S + Q_T \quad (4)$$

Description: $Q_{Total}$ = total reactive power (VAR)
$Q_R$ = reactive power of phase R (VAR)
$Q_S$ = reactive power of phase S (VAR)
$Q_T$ = reactive power of phase T (VAR)

### 2.3. Apparent Power

Apparent power is the trigonometric combination of active power and reactive power and is denoted by S. Its unit is volt-ampere (VA) [12]. In the per-phase measurement, the apparent power can be calculated using the following equation:

$$S = V \,.\, I \quad (5)$$

Description: S = apparent power per phase (VA)
V = voltage (V)
I = current (A)

The total apparent power is obtained from the sum of the apparent power of each phase, as shown in the following equation:

$$S_{Total} = S_R + S_S + S_T \quad (6)$$

Description: $S_{Total}$ = total apparent power (VA)
$S_R$ = apparent power of phase R (VA)
$S_S$ = apparent power of phase S (VA)
$S_T$ = apparent power of phase T (VA)

### 2.4. Power Factor

The effectiveness of electrical energy utilization in a system strongly depends on the correlation between the current and voltage. The phase angle represents the phase difference between the current and voltage, and the cosine of this angle is defined as the power factor (cos φ). Mathematically, the power factor is the ratio of active power to apparent power, which indicates the efficiency of energy use. This angle also indicates the leading or lagging conditions between the voltage and current waveforms. In power systems, the power factor is maintained as close as possible to unity to optimize operational efficiency [13].

### 2.5. Capacitor Bank

A capacitor bank is a parallel arrangement of several capacitor units designed to improve the power quality through power factor correction (cos φ). This device operates based on the compensation principle, where the capacitive characteristic of the capacitor bank neutralizes the inductive characteristic produced by the load. Before the capacitor bank implementation, all active power (kW) and reactive power (kVAR) requirements were supplied directly by the distribution transformer, resulting in a high apparent power demand (kVA). With this system installed, most of the reactive power required by inductive loads is supplied locally by the capacitor bank, allowing the transformer capacity to focus more on supplying active power [14].

### 2.6. PZEM-004T Sensor

Figure 1. PZEM-004T sensor

The PZEM-004T sensor is a multifunctional electrical measurement instrument that supports voltage, current, active power, frequency, energy, and power factor readings through a TTL interface. This module is available in two variants: a 10 A model with a built-in shunt and a 100 A model using an external current transformer. For data communication, the sensor uses four main connection lines (5V, RX, TX, and GND), which require a stable power supply to integrate properly with a microcontroller-based control system [15].

### 2.7. Arduino Mega 2560

Arduino Mega 2560 is a microcontroller board based on the ATmega2560, developed within the Arduino ecosystem as an open-source platform designed to simplify the development of electronics and Internet of Things (IoT) projects. This board provides many pins, including 54 I/O pins (15 of which support PWM), 16 analog inputs, and four UART ports. It supports USB connectivity, has an ICSP header and reset button, and can be powered through a computer USB port or an AC-DC adapter, making it suitable for projects requiring complex input/output configurations [16].

Figure 2. Arduino Mega 2560

### 2.8. ESP32

The ESP32 is a system-on-chip (SoC) microcontroller that integrates Wi-Fi and Bluetooth connectivity in a single module. Developed by Espressif Systems [17], this device is designed for industrial requirements with operational reliability over a wide temperature range (-40°C to +125°C). The main advantage of the ESP32 lies in its power efficiency through clock gating and dynamic power scaling features, making it suitable for Internet of Things (IoT) applications. With highly integrated internal components, such as antennas and power management circuitry, the ESP32 can minimize the use of external PCB components and can be used flexibly as a standalone controller or as a slave device through SPI, I2C, or UART communication interfaces.


Corresponding Author: fandimuhammadyt@gmail.com
Doi : 10.30996/elsains.v8i1.133178

Figure 3. ESP32

### 2.9. *MIT App Inventor*

The MIT App Inventor is an intuitive visual programming software designed to help users develop fully functional applications for Android and iOS devices. This platform uses a block-based programming system that enables users to develop applications without the need to write conventional code.

Previous research [18] showed that MIT App Inventor was used to display monitoring data from environmental sensors such as temperature and humidity sensors (DHT11), ultrasonic sensors for water level measurement, and rain sensors. The data from these sensors were sent through a Wemos D1 R1 microcontroller with ESP8266-based Wi-Fi connectivity and forwarded to the Blynk server. The application developed using MIT App Inventor retrieved data from the Blynk server through an API and displayed it on the user's smartphone.

### 2.10. *Firebase*

Firebase is a cloud-based application development platform that provides various backend-as-a-service (BaaS) features to facilitate the real-time development and management of web and mobile applications. Firebase has several key advantages that make it widely used in modern application development. One of these advantages is real-time data synchronization across devices through the real-time database feature, which allows data from IoT devices to be sent, received, and updated instantly. The integration of IoT devices with mobile or web applications is also simplified through SDK and API support. Firebase also provides authentication features that facilitate user access management, ensuring that only authorized users can monitor or control specific devices. Thus, the application becomes more secure in terms of control and privacy [19].

### 2.11. *Internet of Things*

The Internet of Things (IoT) is an integrated ecosystem that continuously extends Internet connectivity to various physical devices. This technology enables physical objects or hardware to communicate, collaborate, and be controlled through an Internet network. IoT integration plays a crucial role in transforming conventional devices into intelligent systems capable of transmitting data in real-time [20].

## 3 Methodology

### 3.1 *Research Stages*

The research stages were arranged systematically to achieve the objective of designing and implementing an Internet of Things (IoT)-based reactive power compensator control system. The research stage flowchart is presented in Figure 4. The study began with a literature review to obtain theoretical foundations related to the power factor, reactive power compensation, capacitor banks, and IoT implementation in electrical systems. The next stage was system design, which included hardware, software, and system workflow design.

The next stage was system implementation, including device assembly and microcontroller programming according to the proposed design. After the system was constructed, system testing was conducted to ensure that all components worked according to their functions and to evaluate the system performance in improving the power factor. The test data were then collected and analyzed to assess the power factor improvement, system response time, and measurement comparison between the sensors and reference instrument. The final stage involved drawing conclusions based on the analysis results.

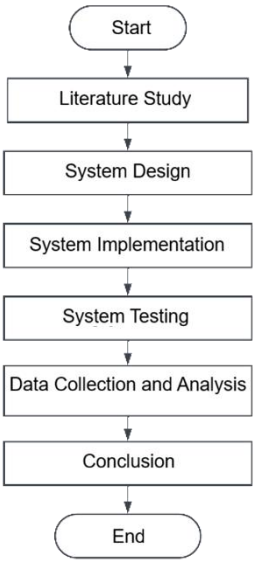


Figure 4. Research stage flowchart

### 3.2 *Block Diagram*

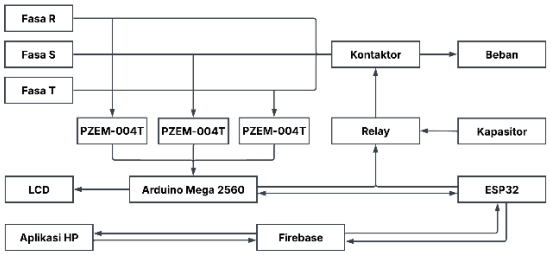


Figure 5. System block diagram

The Internet of Things (IoT)-based three-phase reactive power compensator system was designed, as shown in Figure 5. Each phase was measured using a PZEM-004T sensor to obtain the electrical parameters in real time. The measurement data were processed using an Arduino Mega 2560 as the main controller to determine the compensation requirements, control capacitor relays, and display electrical parameter information on an LCD for local monitoring. Arduino Mega 2560 also communicates with ESP32, which functions as the IoT communication medium that sends data to Firebase so that the system can be monitored and controlled through an Android application.

### 3.3 *Wiring Diagram*

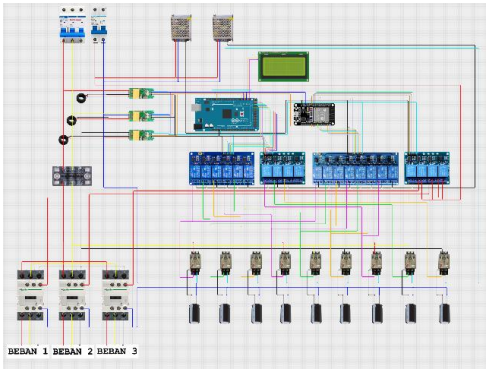


Figure 6. System wiring diagram

The overall reactive power compensation system design is represented by the wiring diagram in Figure 6. The system starts from the power source connected to a three-phase Miniature Circuit Breaker (MCB), which functions as protection and as the main supply distributor to the three-phase load. In addition, a single-phase MCB is used to supply and protect the control circuit and the single-phase loads. The output of the three-phase MCB was distributed to the PZEM-004T sensors installed on phases R, S, and T. Each sensor was connected to a current transformer (CT) to detect the current in each phase in real time, allowing electrical parameters such as voltage, current, active power, reactive power, and power factor to be measured.

The measurement data from the three PZEM-004T sensors were sent to the Arduino Mega as the main data acquisition and processing unit. Arduino Mega processes the data to determine the reactive power compensation requirement for each phase. In addition to serving as the processing center, the Arduino Mega also automatically controls the compensator system and displays electrical parameter information through an I2C-based LCD module installed in the control circuit.

The power supply system uses two switching power supplies that convert the AC voltage to DC voltage. A 5 V power supply was used for the control circuit, including the Arduino Mega, ESP32, SRD5VDC relay module, and LCD. A 24 V power supply was used to supply the LY2N relays, which acted as an interface between the control relay and capacitor power circuit.

The capacitor and load control were performed using SRD5VDC relay modules with 21 channels. These relay modules were divided into two main groups: the first group consisted of nine automatic capacitor relays directly connected to an Arduino Mega. These relays operate based on the calculation of the reactive power compensation requirements. When the SRD5VDC relay is activated, the signal energizes the LY2N relay coil, allowing the capacitor to be connected to the phase requiring compensation.

The second group consists of nine manual capacitor relays and three load control relays connected to the ESP32. These relays allow users to manually control the capacitors and loads using a mobile application. Activating a capacitor relay energizes the LY2N relay to connect the capacitor to a specific phase, whereas activating a load relay energizes the contactor coil so that the load can be connected to or disconnected from the system.

On the actuator side, three contactors are used as electromagnetic switches to connect or disconnect the three-phase load according to the commands from the control system. These contactors ensure safe and reliable load control.

Capacitors, as the main elements of reactive power compensation, are arranged in parallel and evenly distributed across each phase. A total of nine capacitors are used, with each phase R, S, and T having three capacitors rated at 6.5 µF, 4.0 µF, and 3.5 µF. This arrangement enables flexible capacitor switching combinations, such that the compensated reactive power can be adjusted gradually according to the system requirements.

The load used in the system testing consisted of fluorescent lamps arranged into three load groups. Load 1 consisted of three 10 W fluorescent lamps, Load 2 consisted of three 20 W fluorescent lamps, and Load 3 consisted of three 40 W fluorescent lamps. These load variations were used to simulate changing load conditions and evaluate the performance of the reactive power compensator system in improving the power factor under different loading levels.

### *3.4 Circuit Flowchart*

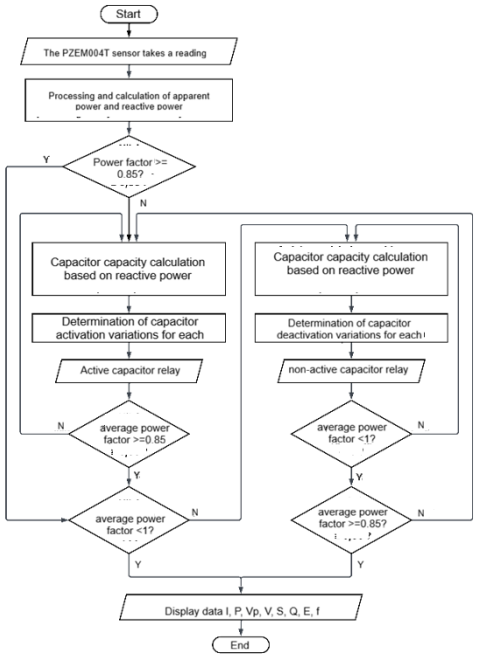


Figure 7. Circuit flowchart

The flowchart in Figure 7 shows the workflow of the Internet of Things (IoT)-based reactive power compensator system. The process begins with electrical parameter readings by the PZEM-004T sensors on each phase, including voltage, current, active power, frequency, energy, and the calculation of apparent and reactive power. These data were then processed using an Arduino Mega 2560 to evaluate the power factor in each phase.

If the detected power factor is ≤ 0.85, the Arduino calculates the required capacitance based on the measured reactive power and determines the capacitor switching variation for each phase. Conversely, if an overcompensation condition occurs with the average power factor exceeding the threshold, the system gradually deactivates the capacitors. The evaluation process was repeated until the average power factor was within the desired operating range. The measurement results were then displayed on an LCD and sent to the IoT platform for monitoring.

### *3.5 Compensation Requirement Calculation Method and Switching Logic*

The reactive power compensation requirement was calculated for each phase based on the active power and power factor measured by the PZEM-004T sensor. The target power factor of the system was set at approximately 0.90, whereas the minimum power factor threshold used to activate the compensator was 0.85. When the power factor in one phase is less than or equal to 0.85, the system calculates the reactive power that must be compensated using the following equation:

$$Q_c = P\,.(tan_{\varphi 1} - tan_{\varphi 2}) \quad (7)$$

Description: $Q_c$ = reactive power compensation (VAR)
P = active power of the load per phase (W)
$\varphi 1$ = phase angle before compensation
$\varphi 2$ = phase angle after compensation

After the reactive power compensation requirement is obtained, the Arduino Mega 2560 determines the most suitable capacitor combination for each phase. The amount of capacitive reactive power supplied by a capacitor is calculated based on the


Corresponding Author: fandimuhammadyt@gmail.com
Doi : 10.30996/elsains.v8i1.133178

capacitance, frequency, and phase voltage using the following equation:

$$Q_C = 2\pi . f . C . V^2 \quad (8)$$

Description: Q_C = capacitive reactive power supplied by the capacitor (VAR)
f = system frequency (Hz)
C = capacitance value (F)
V = phase voltage (V)

Each phase is equipped with three capacitors rated at 6.5, 4.0, and 3.5 µF. The system evaluates seven candidate capacitor combinations, namely, C1, C2, C3, C1+C2, C1+C3, C2+C3, and C1+C2+C3. The selected combination is the one whose capacitive reactive power is closest to the compensation requirement and can increase the power factor toward the target without causing overcompensation. After the capacitor relay is activated, the system again reads the power factor. If the power factor remained below 0.85, the calculation and capacitor selection process was repeated. Conversely, if the power factor shows a tendency toward overcompensation, the system gradually deactivates the capacitors and re-evaluates the condition until the power factor returns to the desired operating range.

### *3.6 Hardware and Software Design*

The hardware design is illustrated in Figure 8. All the device components were arranged and mounted on a board to facilitate the observation, testing, and visual documentation of the system.

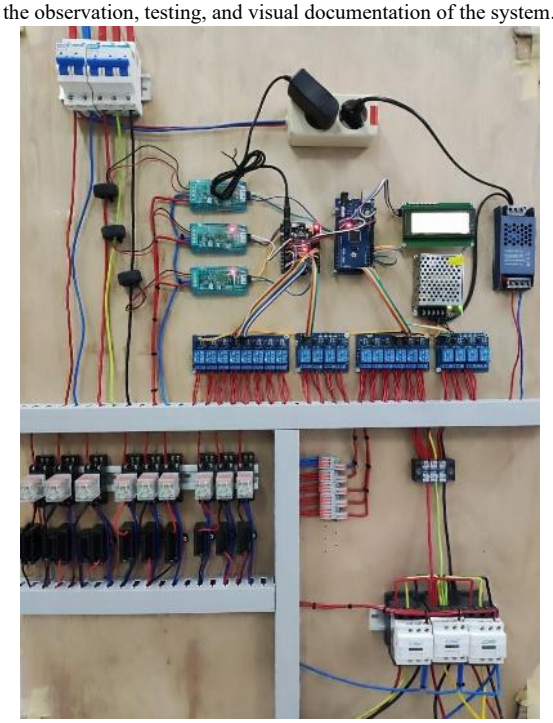

Figure 8. System hardware design

The software design is illustrated in Figure 9. The software was designed as an Android-based user interface that displayed the electrical condition of the system and supported remote device control. The application displays electrical parameters and system status in real time and provides visual monitoring features to help users understand the performance of the reactive power compensator.

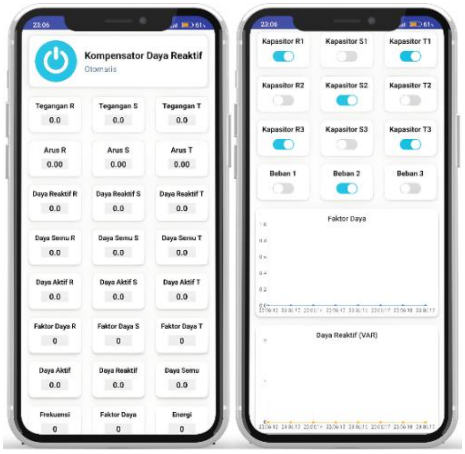


Figure 9. Software application design

### *3.7 System Testing*

Testing was performed using inductive loads in the form of fluorescent lamps configured as balanced three-phase loads. Each load group consisted of three lamps with the same power rating, installed on phases R, S, and T. Load 1 consisted of three 10 W fluorescent lamps, Load 2 consisted of three 20 W fluorescent lamps, and Load 3 consisted of three 40 W fluorescent lamps. Thus, for each load variation, every phase received the same type and power of load. Testing was carried out on a low-voltage three-phase system, with electrical parameters measured per phase using PZEM-004T sensors on phases R, S, and T. System testing was conducted to evaluate the performance of the designed IoT-based three-phase reactive power compensator. The testing focused on the system's ability to improve the power factor, respond to load changes, and display monitoring data in real time. The testing process compared the system conditions before and after compensation under several load variations. The tested parameters included the power factor, system response time, and measurement comparison between the sensor readings and a conventional measuring instrument.

## 4 Discussion

### *4.1 Power Factor Correction Test*

A power factor correction test was conducted to evaluate the ability of an Internet of Things (IoT)-based reactive power compensator system to improve the power factor quality under a three-phase inductive load. The test compared the system conditions before and after compensation for several load variations.

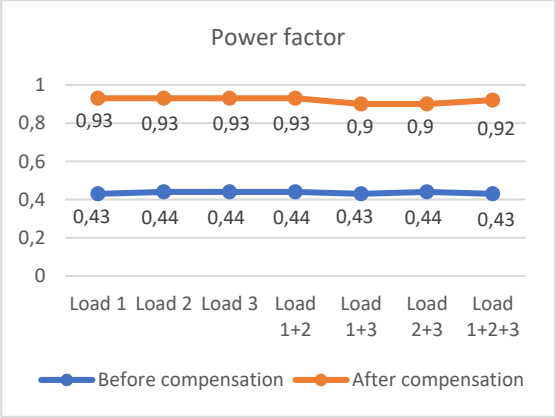


Figure 10. Power factor comparison before and after compensation

The test results in Figure 10 show that before compensation, the power factor ranged from 0.43 to 0.44, indicating the dominance of inductive and reactive power in the system. This

condition causes a relatively large reactive power flow, which reduces the electrical system efficiency. After the compensator system was activated, the power factor increased significantly to the range of 0.90–0.93. This improvement shows that the automatically controlled capacitor bank effectively compensated for the inductive reactive power.

Power factor correction occurs because the system can adjust the activated capacitor combination based on the measured reactive power in each of the three phases. The compensation process is performed gradually until the power factor reaches the desired threshold without causing overcompensation. This indicates that the implemented control algorithm can maintain system stability while improving the electrical energy efficiency.

### *4.2 Automatic Compensation Test*

An automatic compensation test was conducted to observe the system's ability to activate capacitors according to the measured reactive power. The compensation process is performed automatically through Arduino control, which calculates the reactive power from the PZEM-004T sensor readings and then activates the capacitor relays on each phase (R, S, and T) as required.

Table 1. Automatic compensation test data

| Active Load | Active Capacitors | PF before | PF after |
|---|---|---|---|
| Load 1 | R2, S2, T2 | 0,43 | 0,93 |
| Load 2 | R3, S3, T3 | 0,44 | 0,93 |
| Load 3 | R1, S2, S3, T2, T3 | 0,44 | 0,93 |
| Load 1 dan 2 | R2, R3, S2, S3, T2, T3 | 0,44 | 0,93 |
| Load 1 dan 3 | R1, R2, S1, S2, T1, T2 | 0,43 | 0,90 |
| Load 2 dan 3 | R1, R2, S1, S2, T1, T2 | 0,44 | 0,90 |
| Load 1, 2, dan 3 | R1, R2, R3, S1, S2, S3, T1, T2, T3 | 0,43 | 0,92 |

In the developed automatic compensator system, each phase (R, S, and T) is equipped with three capacitors rated at 6.5 µF (R1, S1, T1), 4.0 µF (R2, S2, T2), and 3.5 µF (R3, S3, T3), which are automatically activated by the Arduino Mega according to the reactive power requirements to achieve a target power factor of approximately 0.90. Based on the test results in Table 1, the system was able to select appropriate capacitor combinations under various load conditions, both single and combined loads, so that the initial power factor in the range of 0.43–0.44 was improved to 0.90–0.93. Under full-load conditions, all the capacitors were activated, and the power factor increased to 0.92. Overall, the automatic compensation system operates adaptively and effectively in improving the power factor to the range of 0.90–0.93, thereby satisfying the minimum SPLN power factor standard (≥0.85) and demonstrating good compensation algorithm performance in maintaining system power quality.

### *4.3 System Response Time Test*

A response time test was conducted to evaluate the ability of the reactive power compensator system to respond automatically to changes in the load conditions. The response time is defined as the time interval from when the system detects a change in the power factor until the capacitor activation or deactivation process is completed.

The test was conducted under three load conditions: static load, dynamic load under under-compensation, and dynamic load under over-compensation. Static load refers to a condition in which the load is relatively constant and does not change significantly during the testing. Dynamic load under compensation occurs when the inductive load increases, so that the power factor falls below the specified threshold, and the system needs to add capacitors. Meanwhile, a dynamic load under overcompensation occurs when the number of active capacitors is excessive, causing the power factor to tend toward leading and requiring the system to deactivate some capacitors.

Table 2. Static load response time

| Load Aktif | Trial no. | | | | | | | |
|---|---|---|---|---|---|---|---|---|
| | 1 | 2 | 3 | 4 | 5 | 6 | 7 | 8 |
| Load 1 | 2 | 2 | 2 | 2 | 2 | 2 | 2 | 2 |
| Load 2 | 2 | 2 | 2 | 2 | 2 | 2 | 2 | 2 |
| Load 3 | 2 | 2 | 2 | 2 | 2 | 2 | 2 | 2 |
| Load 1 dan 2 | 2 | 3 | 2 | 2 | 2 | 3 | 2 | 2 |
| Load 1 dan 3 | 8 | 8 | 7 | 7 | 8 | 7 | 8 | 8 |
| Load 2 dan 3 | 8 | 9 | 8 | 7 | 8 | 6 | 7 | 6 |
| Load 1, 2, dan 3 | 5 | 5 | 6 | 5 | 5 | 6 | 6 | 5 |

Based on Table 2, the system response time under static load conditions ranged from 2 s to 9 s. The fastest response occurred in the single-load tests, namely Loads 1, 2, and 3, with a consistent response time of 2 s. Meanwhile, the longest response time occurred in the Load 2 and Load 3 combination, reaching 9 s. This difference in response time was influenced by the number of capacitor combinations that had to be evaluated by the system to achieve the target power factor.

Table 3. Under-compensation load response time

| Active Load | Trial no. | | | | | |
|---|---|---|---|---|---|---|
| | 1 | 2 | 3 | 4 | 5 | 6 |
| B0 → B1 | 8 | 7 | 8 | 8 | 9 | 8 |
| B0 → B2 | 10 | 9 | 12 | 11 | 10 | 10 |
| B0 → B3 | 8 | 9 | 9 | 10 | 11 | 8 |
| B1 → B1 + B2 | 10 | 10 | 11 | 9 | 10 | 11 |
| B2 → B1 + B2 | 11 | 10 | 11 | 10 | 10 | 10 |
| B3 → B2 + B3 | 8 | 7 | 7 | 7 | 8 | 6 |
| B1+B2 → B1+B2+B3 | 8 | 8 | 7 | 7 | 9 | 8 |
| B1+B3 → B1+B2+ B3 | 6 | 7 | 6 | 6 | 7 | 6 |
| B2+B3 → B1+B2+B3 | 9 | 8 | 9 | 7 | 7 | 8 |

Based on Table 3, the system response time under dynamic under-compensation conditions ranged from 6 s to 12 s. The fastest response occurred in the B3 → B2+B3 and B1+B3 → B1+B2+B3 transitions at 6 s. The longest response occurred in the B0 → B2 transition at 12 s. This condition shows that load addition requires the system to detect a decrease in the power factor, calculate the compensation requirement, and activate the appropriate capacitor combination.

Table 4. Over-compensation load response time

| Active Load | Trial no. | | | | | |
|---|---|---|---|---|---|---|
| | 1 | 2 | 3 | 4 | 5 | 6 |
| B1+B2+B3→ B1+B2 | 8 | 7 | 7 | 8 | 7 | 7 |
| B1+B2+B3→ B1+B3 | 16 | 15 | 15 | 16 | 14 | 15 |
| B1+B2+B3→ B2+B3 | 15 | 15 | 15 | 16 | 16 | 14 |
| B1+B2 → B1 | 6 | 6 | 7 | 8 | 6 | 6 |
| B1+B2 → B2 | 5 | 6 | 5 | 5 | 7 | 5 |
| B2+B3 → B3 | 8 | 7 | 7 | 7 | 8 | 9 |
| B1 → B0 | 1 | 1 | 1 | 1 | 1 | 1 |
| B2 → B0 | 1 | 1 | 1 | 1 | 1 | 1 |
| B3 → B0 | 1 | 1 | 1 | 1 | 1 | 1 |

Based on Table 4, the system response time under overcompensation conditions ranged from 1 to 16 s. The fastest response occurred during the transitions to the no-load conditions, namely B1 → B0, B2 → B0, and B3 → B0, with a response time of 1 s. This occurred because the system only needed to deactivate the capacitors. The longest response occurred in the B1+B2+B3 → B1+B3 and B1+B2+B3 → B2+B3 transitions, reaching 16 s. The longer response time in these transitions was caused by the


Corresponding Author: fandimuhammadyt@gmail.com
Doi : 10.30996/elsains.v8i1.133178

process of deactivating excess capacitors, re-reading the power factor, and selecting the capacitor combination suitable for the final load condition.

*4.4 Monitoring System Comparison Test*

Figure 11. Lutron DW-6095 measurement display

This test was performed to evaluate the agreement between the readings of an Internet of Things (IoT)-based monitoring system and a reference instrument. The test compared the electrical parameter readings from the PZEM-004T sensor with those measured using the Lutron DW-6095 power meter analyzer. The parameters compared included voltage (V), current (A), and power factor (PF). The difference and error were calculated using the following equations:

$$Difference = PZEM\ Result - Lutron\ Result \quad (9)$$

$$Error = \frac{PZEM\ Result - Lutron\ Result}{Lutron\ Reult} \times 100\% \quad (10)$$

The results of the comparison of the monitoring systems are presented in Tables 5, 6, and 7.

Table 5. Voltage measurement comparison

| Voltage Lutron DW-6095 | Voltage PZEM-004T | Difference (V) | Error (%) |
|---|---|---|---|
| 230,9 | 231,8 | 0,9 | 0,39% |
| 231,0 | 231,9 | 0,9 | 0,39% |
| 232,8 | 233,6 | 0,8 | 0,34% |
| 232,2 | 233,3 | 1,1 | 0,47% |
| 234,0 | 234,7 | 0,7 | 0,30% |
| 233,2 | 233,6 | 0,4 | 0,17% |
| 232,1 | 233,0 | 0,9 | 0,39% |
| 230,2 | 231,0 | 0,8 | 0,35% |
| 230,4 | 231,2 | 0,8 | 0,35% |
| 231,7 | 232,6 | 0,9 | 0,39% |

Based on Table 5, the voltage measurements from the PZEM-004T sensor showed relatively small differences compared with those of the Lutron DW-6095 reference instrument. The voltage difference ranged from 0.4 to 1.1 V, with a percentage error of 0.17 to 0.47%. These results indicate that the voltage readings from the PZEM-004T were close to those of the reference instrument

Table 6. Current measurement comparison

| Current Lutron DW-6095 | Current PZEM-004T | Difference (A) | Error (%) |
|---|---|---|---|
| 0,32 | 0,31 | 0,01 | 3,1% |
| 0,35 | 0,35 | 0,0 | 0,0% |
| 1,33 | 1,32 | 0,01 | 0,8% |
| 0,31 | 0,34 | 0,03 | 9,7% |
| 0,37 | 0,36 | 0,01 | 2,7% |
| 0,49 | 0,46 | 0,03 | 6,1% |
| 0,32 | 0,31 | 0,01 | 3,1% |
| 0,33 | 0,30 | 0,03 | 9,1% |
| 0,67 | 0,67 | 0,0 | 0,0% |
| 0,52 | 0,49 | 0,03 | 5,8% |

Based on Table 6, the current measurements showed differences of 0.00 to 0.03 A compared with those of the Lutron DW-6095. In percentage terms, the current measurement error ranged from 0.0 to 9.7%. The largest percentage error occurred under low-current conditions; therefore, a small absolute difference still resulted in a larger percentage error.

Table 7. Power factor measurement comparison

| Power factor Lutron DW-6095 | Power factor PZEM-004T | Power factor Difference | Error (%) |
|---|---|---|---|
| 0,41 | 0,42 | 0,01 | 2,4% |
| 0,43 | 0,43 | 0,0 | 0,0% |
| 0,90 | 0,91 | 0,01 | 1,1% |
| 0,90 | 0,93 | 0,03 | 3,3% |
| 0,93 | 0,93 | 0,0 | 0,0% |
| 0,90 | 0,92 | 0,02 | 2,2% |
| 0,42 | 0,43 | 0,01 | 2,4% |
| 0,85 | 0,86 | 0,01 | 1,2% |
| 0,40 | 0,42 | 0,02 | 5,0% |
| 0,91 | 0,93 | 0,02 | 2,2% |

Based on Table 7, the power factor readings from the PZEM-004T sensor showed differences of 0.00 to 0.03 compared with those of the Lutron DW-6095. The power factor percentage error ranged from 0.0 to 5.0%. These results indicate that the PZEM-004T-based monitoring system can provide power factor readings close to those of the reference instrument under the tested conditions.

## 5 Conclusion

Based on the design, testing, and discussion results, it can be concluded that the developed Internet of Things (IoT)-based three-phase reactive power compensator system can improve the power factor automatically and in real time. The test results show that the power factor, initially in the range of 0.43 to 0.44, can be improved to 0.90 to 0.93 after activating the compensator system. The system response time was 2 to 9 s under static load testing, 6 to 12 s under dynamic under-compensation testing, and 1 to 16 s under dynamic over-compensation testing. In addition, the comparison between the IoT-based monitoring system and the conventional Lutron DW-6095 measuring instrument showed differences of 0.4 to 1.1 V for voltage measurement, 0.00 to 0.03 A for current measurement, and 0.00 to 0.03 for power factor measurement. The percentage error ranges were 0.17–0.47% for voltage, 0.0–9.7% for current, and 0.0–5.0% for power factor. The largest current error occurred under low-current conditions, although the current difference was relatively small. A limitation of this study is that testing was conducted at the laboratory scale using balanced three-phase fluorescent lamp loads; therefore, further testing with more varied industrial loads is needed to evaluate the system performance under more complex operating conditions.

## Author Contribution

Conceptualization, Author 1 and Author 2; methodology, Author 1; software, Author 1; validation, Author 1, Author 2, Author 3, and Author 4; formal analysis, Author 1; investigation, Author 1 and Author 2; resources, Author 1 and Author 2; data curation, Author 1; writing—original draft preparation, Author 1; writing—review and editing, Author 2, Author 3, and Author 4; visualization, Author 1; supervision, Author 2; project administration, Author 1 and Author 2.

## Acknowledment

The authors thank all parties who provided support and contributed to the implementation of this research. In particular, the authors express their appreciation to the supervisors for their guidance, direction, and input during the research and manuscript preparation process. The authors also thank the examiners for their constructive suggestions and evaluations for improving this research. The authors also thank Universitas Negeri Surabaya and the D4 Electrical Engineering laboratory for providing the

Corresponding Author: fandimuhammadyt@gmail.com

Doi : 10.30996/elsains.v8i1.133178

facilities and supporting resources that enabled this research to be completed.

## Reference

[1] Sugianto and P. Untara, "Studi Susut Energi pada Sistem Distribusi Tenaga Listrik Melalui Analisis Pengukuran dan Perhitungan," *Sinusoida*, vol. XXI, Apr. 2019, doi: 10.37277/s.v21i2.686.

[2] T. Sukendar, R. Sinambela, M. Awaludin, and A. G. Gani, "Analisa Faktor Daya Menggunakan Capacitor Bank untuk Meningkatkan Kualitas Daya Listrik di Wisma Nusantara Internasional", doi: 10.35968/jsi.v11i2.1259.

[3] B. Ferdiansah, A. Margiantono, and F. Ahmad, "Analisis Pengaruh Kapasitor Bank Terhadap Nilai Faktor Daya dan Nilai Jatuh Tegangan," *Jambura Journal of Electrical and Electronics Engineering*, vol. 5, Jul. 2023, doi: 10.37905/jjeee.v5i2.20893.

[4] P. ANGGA JULIANTARA, I. W. ARTA WIJAYA, and C. G. INDRA PARTHA, "Rancang Bangun Kapasitor Bank Otomatis Berbasis Mikrokontroler ATmega 328P Untuk Perbaikan Faktor Daya," *Jurnal SPEKTRUM*, vol. 5, pp. 157–163, Jun. 2018, doi: 10.24843/SPEKTRUM.2018.v05.i01.p23.

[5] R. N. Prasetyono, R. Mubarok, R. C. Sigitta, M. Z. Alfarikhi, N. Nasrulloh, and R. A. Murdiantoro, "Pengaruh Penambahan Kapasitor Bank terhadap Perbaikan Daya pada Direct On Line (DOL) Berbasis Programmable Logic Controller (PLC) di Motor Listrik 3 Phase," *Journal of Telecommunication Electronics and Control Engineering (JTECE)*, vol. 5, no. 2, pp. 132–143, Jul. 2023, doi: 10.20895/jtece.v5i2.1066.

[6] R. Harahap and Y. M. Lumban Toruan, "Rancang Bangun Kapasitor Bank Otomatis Untuk Perbaikan Faktor Daya Pada Motor Induksi Tiga Fasa Berbasis Arduino Uno," *JET (Journal of Electrical Technology)*, vol. 6, Jun. 2023, doi: 10.30743/jet.v8i2.7679.

[7] F. Farid and N. S. Salahuddin, "Sistem Pantau dan Kendali Peralatan Listrik Rumah Berbasis *Internet of Things* (*IoT*)," *G-Tech: Jurnal Teknologi Terapan*, vol. 8, no. 2, pp. 1079–1090, Apr. 2024, doi: 10.33379/gtech.v8i2.4089.

[8] I. Surya *et al.*, "Sistem *monitoring* beban listrik dan perbaikan faktor daya menggunakan PZEM-004T dan dashboard Adafruit berbasis *IoT*," *JITEL (Jurnal Ilmiah Telekomunikasi, Elektronika, dan Listrik Tenaga)*, vol. 3, no. 3, pp. 235–246, Sep. 2023, doi: 10.35313/jitel.v3.i3.2023.235-246.

[9] F. Setiawan, A. Wasono, and E. A. Kurniawan, "Rancang Bangun Kapasitor Bank Otomatis untuk Mengetahui Dampak terhadap Kualitas Daya Listrik pada Variasi Beban Pelanggan 5500VA," *ORBITH*, vol. 21, pp. 51–56, Mar. 2025, doi: 10.32497/orbith.v21i1.5906.

[10] A. Tama, E. A. Yulanda, S. Sunardi, K. A. Wirakusuma, and P. B. Laksono, "Analisis Pengaruh Perubahan Arus Eksitasi Terhadap Tegangan Keluaran dan Daya Reaktif di PLTG Gilimanuk," *EPIC Journal of Electrical Power Instrumentation and Control*, vol. 7, no. 1, pp. 1–10, Jun. 2024, doi: 10.32493/epic.v7i1.38427.

[11] A. Dani and M. Hasanuddin, "Perbaikan faktor daya menggunakan kapasitor sebagai kompensator daya reaktif (studi kasus STT Sinar Husni)," *Seminar Nasional Royal (SENAR)*, vol. 1, pp. 673–678, 2018.

[12] J. Murianto, D. Febrianto, Wandy, F. Azmi, and D. Perangin-angin, "Rancang Bangun Alat Uji Pada Perbaikan Faktor Daya Dengan Kapasitor Bank," *JESCE (Journal of Electrical and System Control Engineering)*, vol. 4, no. 1, pp. 53–62, Aug. 2020, doi: 10.31289/jesce.v4i1.3995.

[13] R. Ferdinand and A. Rofii, "ANALISA PENGGUNAAN KAPASITOR BANK DALAM UPAYA PERBAIKAN FAKTOR DAYA," *Ejournal Kajian Teknik Elektro*, vol. 3, Mar. 2018, doi: 10.52447/jkte.v3i1.1056.

[14] I. Hajar, S. Megi Rahayuni, and I. Artikel, "Analisis Perbaikan Faktor Daya Menggunakan Kapasitor Bank Di Plant 6 PT. Indocement Tunggal Prakarsa Tbk. Unit Citeureup," *Jurnal Ilmiah Setrum*, vol. 9, no. 1, pp. 8–16, 2020, doi: 10.36055/setrum.v9i1.8111.

[15] S. Anwar, T. Artono, and J. Teknik Elektro Politeknik Negeri Padang, "Pengukuran Energi Listrik Berbasis PZEM-004T," *Proceeding Seminar Nasional Politeknik Negeri Lhokseumawe*, vol. 3, no. 1, 2019.

[16] D. Sasmoko, *Arduino dan Sensor Pada Project Arduino DIY*. Semarang: Yayasan Prima Agus Teknik, 2021.

[17] Espressif Systems, "ESP32 Series Datasheet," Espressif Systems, 2025. [Online]. Available: https://documentation.espressif.com/esp32_datasheet_en.pdf. Accessed: Jan. 13, 2026.

[18] M. bahrul Ulum and F. Badri, "SISTEM *MONITORING* CUACA DAN PERINGATAN BANJIR BERBASIS *IOT* DENGAN MENGGUNAKAN APLIKASI MIT APP INVENTOR," *Jurnal Informatika dan Teknik Elektro Terapan*, vol. 11, no. 3, Aug. 2023, doi: 10.23960/jitet.v11i3.3088.

[19] Google Firebase, "Firebase Realtime Database," Firebase Documentation, 2026. [Online]. Available: https://firebase.google.com/docs/database. Accessed: Jan. 13, 2026.

[20] Ayu Syahfitri, "*Internet of Things* (*IoT*), Sejarah, Teknologi, dan Penerapannya," *Uranus : Jurnal Ilmiah Teknik Elektro, Sains dan Informatika*, vol. 3, no. 1, pp. 113–120, Jan. 2025, doi: 10.61132/uranus.v3i1.667.


Corresponding Author: fandimuhammadyt@gmail.com
Doi : 10.30996/elsains.v8i1.133178